Charge and quadrupole fluctuations and gap anisotropy in BiS_2-based superconductors

Katsuhiro Suzuki,[1] Hidetomo Usui,[2] Kazuhiko Kuroki,[2] and Hiroaki Ikeda[3]
[1]*Research Organization of Science and Technology, Ritsumeikan University, Kusatsu, Shiga 525-8577, Japan*
[2]*Department of Physics, Osaka University, Toyonaka, Osaka 560-0043, Japan*
[3]*Department of Physics, Ritsumeikan University, Kusatsu, Shiga 525-8577, Japan*
(Received 5 March 2017; published 21 July 2017)

Recent angle-resolved spectroscopy in BiS_2-based superconductors has indicated that the superconducting gap amplitude possesses remarkable anisotropy and/or a sign change on a small Fermi pocket around the X point. It implies a possibility of an unconventional pairing state. Here we study the gap anisotropy in superconductivity mediated by inherent charge and quadrupole fluctuations in an extended Hubbard model, which includes intersite interaction between Bi and S atoms. The first-principles downfolded band structure is composed of Bi $6p_x/p_y$ and S $3p_x/p_y$ orbitals on a BiS_2 single layer. Evaluating the linearized gap equation, we find that the ferroic charge and quadrupole fluctuation driven by the intersite interaction leads to a fully gapped $d_{x^2-y^2}$-wave pairing state, in which the gap amplitude has sizable anisotropy on the Fermi surface.

DOI: 10.1103/PhysRevB.96.024513

I. INTRODUCTION

Recently discovered BiS_2-based layered superconductors, $Bi_4O_4S_3$ [1] and $LnO_{1-x}F_xBiS_2$ (Ln = lanthanide) [2–6], have attracted great interest as the related materials of iron-based superconductors [7]. The highest transition temperature $T_c = 10.6$ K is observed in $LaO_{0.5}F_{0.5}BiS_2$ [2]. The parent material $LaOBiS_2$ is semiconducting and possesses a crystal structure with alternating stacking of BiS_2 twin layers and LnO insulating blocking layers. Superconductivity emerges via electron doping by substituting O with F. Owing to the layered structure, the electronic structure is two dimensional, and the BiS_2 twin layers become conductive with electron doping. The electronic band constructing the Fermi surface is mainly composed of the Bi $6p_x$ and $6p_y$ orbitals. Therefore, it is expected that these orbitals have a relatively large spin-orbit coupling [8]. Moreover, due to the nonsymmorphic space group, the BiS_2 twin layers locally break the inversion symmetry at a Bi site. These features, shared with superconductors with a zigzag chain, CrAs [9] and UCoGe [10], are also fascinating in terms of noncentrosymmetric superconductors [11].

Concerning the pairing state and mechanisms, two possibilities, i.e., the conventional s wave mediated by the electron-phonon interaction [12–14] and unconventional superconductivity driven by the purely electronic interactions [15–21], have been theoretically investigated in the early stage of the study [22]. Experimentally, there is no strong evidence of the electron correlation effect. Measurements of penetration depth and thermal conductivity indicate that $NdO_{0.7}F_{0.3}BiS_2$ is a fully gapped superconductor [23,24]. These observations imply that the superconducting pairing mechanism in this system is the conventional phononic mechanism. However, recent measurements of field-angle-dependent Andreev reflection spectroscopy [25] and muon spin relaxation [26] have reported that the superconducting gap amplitude is highly anisotropic. Also, angle-resolved photoemission spectroscopy (ARPES) [27] has indicated the presence of remarkable anisotropy and/or a possibility of sign change of the superconducting gap on a small Fermi pocket around the X point. These observations imply a possibility of an unconventional pairing mechanism in this superconductor. In general, such anisotropic gap structure needs an unconventional mechanism, for instance, strongly k-dependent fluctuations, or two kinds of competitive forces, such as electron-phonon attractive force and electron repulsive force. In addition, the observation of a "checkerboard-stripe" pattern in scanning tunneling microscopy/scanning tunneling spectroscopy (STM/STS) measurements [28] is indicative of the importance of charge/orbital fluctuations.

Here, to clarify this point, we study in detail a gap anisotropy of unconventional superconductivity induced by purely electronic repulsive forces. First of all, we perform the first-principles calculations [29] of $LaOBiS_2$ without the spin-orbit coupling. Next, we construct a downfolded eight-band tight-binding Hamiltonian by using the maximally localized Wannier functions (MLWFs) [30,31]. The target band consists of $6p_x/p_y$ orbitals of two Bi atoms and $3p_x/p_y$ orbitals of two in-plane S atoms in the unit cell. Furthermore, by neglecting small interlayer hopping integrals, the eight-orbital model is reduced to be the four-orbital model in a single BiS_2 layer. We elucidate charge/orbital fluctuations in this four-orbital model for electron doping corresponding to $x = 0.3$ within the random phase approximation (RPA). As the purely electronic interactions, in addition to the conventional Hubbard-type on-site Coulomb interactions, we consider intersite interactions between Bi and S atoms. We find that the intersite interactions enhance a ferroic charge fluctuation; in particular, orbital-dependent intersite interactions lead to a ferroic quadrupole fluctuation. This may be consistent with the checkerboard stripe observed in STM/STS [28]. Furthermore, solving the superconducting gap equation, we find the possibility of a fully gapped $d_{x^2-y^2}$-wave (B_{1g}) pairing state mediated by such charge and quadrupole fluctuations. The gap amplitude on the Fermi surface has sizable anisotropy, which is similar to the experimental observations. Finally, we realize that the intersite interactions between Bi and S atoms are the key ingredients to understand the superconductivity of this material, although it may be difficult to understand it in terms of purely electronic interactions.

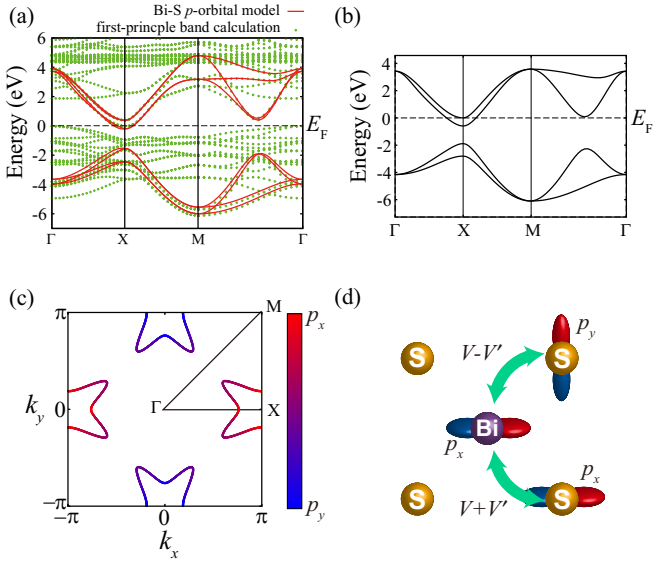

FIG. 1. (a) Band structure obtained by the first-principles calculation of $LaOBiS_2$ (green dots) and a downfolded eight-orbital model (red line). (b) Band structure in our four-orbital model, and (c) the Fermi surface colored by the weight of Bi $6p_x$ (red) and $6p_y$ (blue). Here, the electron filling corresponds to $x = 0.3$. (d) Schematic diagram of intersite interactions between Bi and S. $V \pm V'$ correspond to intra-/interorbital interactions.

II. MODEL HAMILTONIAN AND RANDOM PHASE APPROXIMATION

The BiS_2-based superconductors have a common feature of two-dimensional Fermi surface, which mainly comes from the Bi $6p$ orbitals. In order to study the characteristic low-energy effective model, we use a downfolded band structure of $LaO_{0.5}F_{0.5}BiS_2$ as in the previous study [16]. We start with the first-principles calculations of $LaO_{0.5}F_{0.5}BiS_2$ using the WIEN2K package [29] with the experimental lattice parameters [2]. We take $RK_{\max} = 7$ and 512 k-points grid, and adopt the generalized-gradient-approximation Perdew-Burke-Ernzerhof (GGA-PBE) exchange-correlation functional [32]. Then, we describe the target bands near the Fermi level based on the MLWFs [30,31] of Bi $6p_x/p_y$ and S $3p_x/p_y$ orbitals. Finally, we obtain an effective eight-orbital tight-binding model considering the BiS_2 twin layer in the unit cell. It well reproduces the original band structure as shown in Fig. 1(a). In the obtained transfer integrals, we find that the interlayer hopping integrals are very small due to the two-dimensional structure. Indeed, we can see in Fig. 1(b) that the four-orbital model without the interlayer hoppings [33], i.e., the BiS_2 single-layer model, relatively well reproduces the band structure near the Fermi level. Note that the Fermi level has been shifted to the level corresponding to F doping $x = 0.3$, not $x = 0.5$. Figure 1(c) depicts the corresponding Fermi surface colored by the weight of Bi $6p_x/p_y$ orbitals, where the x/y direction corresponds to a Bi-Bi direction, rotating by 45 degree from X/Y in the previous study [16].

Here we consider as usual the Hubbard-type interactions on the Bi site,

$$\mathcal{H}_I^{\text{intra}} = \sum_i \Big[\sum_\nu U n_{i\nu\uparrow} n_{i\nu\downarrow} + \sum_{\mu>\nu} U' n_{i\nu} n_{i\mu} + \sum_{\mu>\nu} J \hat{S}_{i\nu} \cdot \hat{S}_{i\mu} + \sum_{\nu\neq\mu} J' c^\dagger_{i\nu\uparrow} c^\dagger_{i\nu\downarrow} c_{i\mu\downarrow} c_{i\mu\uparrow} \Big], \quad (1)$$

with

$$n_{i\nu} = \sum_\sigma n_{i\nu\sigma} = \sum_\sigma c^\dagger_{i\nu\sigma} c_{i\nu\sigma},$$
$$\hat{S}_{i\nu} = \sum_{\alpha\beta} c^\dagger_{i\nu\alpha} \hat{\sigma}_{\alpha\beta} c_{i\nu\beta},$$

where $\hat{\sigma}$ is the Pauli matrices, and $c_{i\nu\sigma}$ is an annihilation operator of a spin-σ electron on the ν orbital (p_x or p_y) at the i site. For simplicity, we fix the ratio of each interaction to the intraorbital repulsion U as follows: $U' = 3U/4$ for the interorbital interaction, and $J = J' = U/8$ for the Hund's coupling J and the pair hopping J'. Here, we neglect the on-site interactions on the S atom. However, this does not affect our results since the partial density of states at the Fermi level is small. Next, considering a wide spread of MLWFs of Bi $6p$ orbitals, we include the intersite interactions $V \pm V'$ between the Bi and S atoms as shown in Fig. 1(d),

$$\mathcal{H}_I^{\text{inter}} = \sum_{\langle i,j\rangle} \sum_{\nu\neq\mu} (V + V') n_{i\nu} n_{j\nu} + (V - V') n_{i\nu} n_{j\mu}, \quad (2)$$

where $\langle i,j\rangle$ denotes a summation for the neighboring Bi and S atoms. Although generally $V' \neq 0$, hereafter, $V' = 0$ unless otherwise noted.

Now, let us investigate what kinds of fluctuations grow in the extended Hubbard model within the RPA. In the present four-orbital model, the spin and charge (orbital) susceptibilities are evaluated through the following 8×8 matrices [34]:

$$\hat{\chi}_{s(c)}(q) = \hat{\chi}_0(q)[\hat{1} - \hat{\Gamma}_{s(c)} \hat{\chi}_0(q)]^{-1}, \quad (3)$$

where $q = (\boldsymbol{q}, i\nu_n)$ with boson Matsubara frequencies ν_n, and $\hat{1}$ is an identity matrix. Each element of the irreducible susceptibility matrix $\hat{\chi}_0(q)$ is obtained from

$$\chi_0^{12,34}(q) = -\frac{T}{N} \sum_k G_0^{13}(k+q) G_0^{42}(k), \quad (4)$$

where labels 1–4 symbolically denote an atom (Bi/S) and its orbital (p_x/p_y) in the unit cell, and $G_0^{13}(k)$ is the one-particle bare Green's function between label 1 and label 3. Moreover, the elements of the bare interaction matrix $\hat{\Gamma}_{s/c}$ are given by

$$\Gamma_s^{12,34} = \begin{cases} S_{\ell_1\ell_2,\ell_3\ell_4} & (1-4 \in \text{Bi}) \\ 0 & (\text{otherwise}), \end{cases} \quad (5)$$

$$-\Gamma_c^{12,34} = \begin{cases} C_{\ell_1\ell_2,\ell_3\ell_4} & (1-4 \in \text{Bi}) \\ V_{\ell_1\ell_2,\ell_3\ell_4}(\boldsymbol{q}) & (1,2 \in \text{Bi and } 3,4 \in \text{S}) \\ V^*_{\ell_1\ell_2,\ell_3\ell_4}(\boldsymbol{q}) & (1,2 \in \text{S and } 3,4 \in \text{Bi}) \\ 0 & (\text{otherwise}), \end{cases} \quad (6)$$

where $\ell_1 - \ell_4$ denotes an orbital p_x/p_y on a Bi/S atom. The on-site Coulomb repulsions $\hat{S}/\hat{C}$ are as usual given by

$$S_{l_1l_2,l_3l_4} = \begin{cases} U & (l_1 = l_2 = l_3 = l_4) \\ U' & (l_1 = l_3 \neq l_2 = l_4) \\ J & (l_1 = l_2 \neq l_3 = l_4) \\ J' & (l_1 = l_4 \neq l_2 = l_3) \\ 0 & \text{(otherwise)}, \end{cases} \tag{7}$$

$$C_{l_1l_2,l_3l_4} = \begin{cases} U & (l_1 = l_2 = l_3 = l_4) \\ 2J - U' & (l_1 = l_3 \neq l_2 = l_4) \\ 2U' - J & (l_1 = l_2 \neq l_3 = l_4) \\ J' & (l_1 = l_4 \neq l_2 = l_3) \\ 0 & \text{(otherwise)}. \end{cases} \tag{8}$$

The additional intersite interactions $\hat{V}(\boldsymbol{q})$ are expressed by

$$V_{ll,mm} = \begin{cases} 2\gamma(\boldsymbol{q})(V + V') & (l = m) \\ 2\gamma(\boldsymbol{q})(V - V') & (l \neq m), \end{cases} \tag{9}$$

where $\ell(m) = p_x/p_y$ and $\gamma(\boldsymbol{q}) = \sum_j \exp(i\boldsymbol{q}\cdot\boldsymbol{R}_j)$, and $\boldsymbol{R}_j$ is a relative coordinate between the neighboring Bi and S atoms $[\boldsymbol{R}_j = (0,0),(0,-1),(-1,0),(-1,-1)]$. In the form of Eq. (3), the Stoner factors in the spin (charge) sectors, $\alpha_{s(c)}$, are defined as the maximum eigenvalue of $\hat{\Gamma}_{s(c)}\hat{\chi}_0(q)$. They are measures of the dominant spin (charge) fluctuations. When they are equal to unity, the corresponding spin or charge (orbital) ordering can be realized.

Finally, we investigate a possible spin-singlet superconductivity mediated by these dominant fluctuations. For this purpose, we evaluate the linearized gap equation [34],

$$\lambda\phi^{56}(\boldsymbol{k}) = -\frac{T}{N}\sum_n\sum_{\boldsymbol{q}}\sum_{1234} V_s^{51,26}(\boldsymbol{q},0)G_0^{13}(\boldsymbol{k}-\boldsymbol{q},i\omega_n) \times \phi^{34}(\boldsymbol{k}-\boldsymbol{q})G_0^{24}(\boldsymbol{q}-\boldsymbol{k},-i\omega_n), \tag{10}$$

with the pairing interaction

$$\hat{V}_s(q) = \frac{1}{2}[\hat{C}(q) + \hat{S}] + \frac{3}{2}\hat{S}\hat{\chi}_s(q)\hat{S} - \frac{1}{2}\hat{C}(q)\hat{\chi}_c(q)\hat{C}(q). \tag{11}$$

Here, $\phi^{12}(\boldsymbol{k})$ is a superconducting gap function between orbitals 1 and 2, and λ is the corresponding eigenvalue, which is unity at $T = T_c$. With the unitary matrix diagonalizing the four-orbital tight-binding term, $\phi^{12}(\boldsymbol{k})$ is transformed into $\Delta(\boldsymbol{k})$ in the band representation. In the present numerical calculations, we fix $T = 0.001$ eV, and used 256×256 k-mesh grid and 1024 Matsubara frequencies.

III. CHARGE AND QUADRUPOLE FLUCTUATIONS AND SUPERCONDUCTIVITY

A. Gap function

First, let us discuss the dominant fluctuations and possible gap structure obtained within the RPA. We start with the case of $V = 0$ and $U = 2.2$ eV. Figure 2(a) depicts the dominant spin/charge fluctuations ($\chi_s^{\max}/\chi_c^{\max}$) along the high-symmetry line. As expected, the magnetic fluctuation χ_s is enhanced, while the charge fluctuation χ_c is not enhanced. The characteristic Q structure of $\chi_s^{\max}$ originates from the Fermi surface nesting. From Eqs. (7) and (8), we calculate possible gap structures in superconductivity mediated by such spin fluctuations. Figures 2(b)–2(d) indicate A_{1g}, B_{1g}, and A_{2g} gap structures, respectively. The leading pairing state is a B_{1g} state in Fig. 2(c) and an A_{2g} state in Fig. 2(d). Eigenvalue $\lambda = 1.31$ of the former is larger than $\lambda = 1.17$ of the latter. The sequence can be easily changed, depending on the electron filling, as already reported in the previous study [15]. Thus, these superconducting states are nearly degenerate.

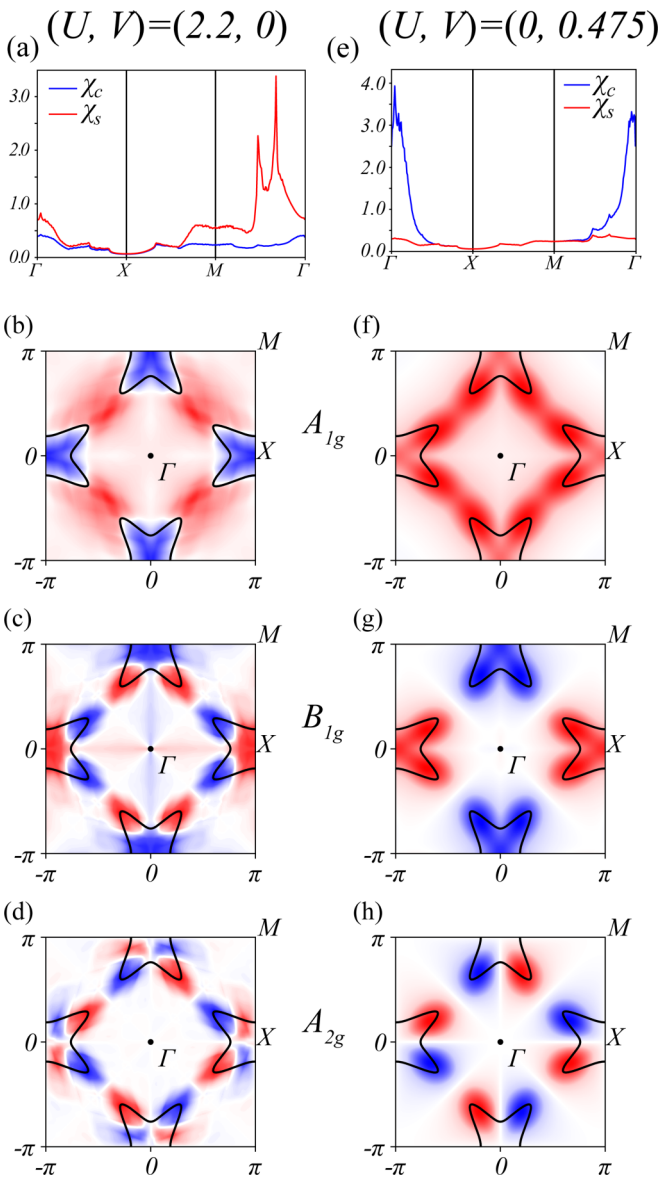

FIG. 2. Charge/spin susceptibility and gap function for each of the symmetries A_{1g}, B_{1g}, and A_{2g} at (a)–(d) $(U,V) = (2.2,0.0)$ eV and (e)–(h) $(U,V) = (0.0,0.475)$ eV.

Next, let us consider the case of $(U,V) = (0.0,0.475)$ eV. We illustrate the dominant fluctuations in Fig. 2(e) and possible gap structures in Figs. 2(f)–2(h). In this case, the spin fluctuations are not enhanced. The dominant fluctuation is a ferroic charge fluctuation. Since the enhanced charge fluctuation favors an isotropic gap on the small Fermi pocket, the fine structure observed in Figs. 2(b)–2(d) is completely or

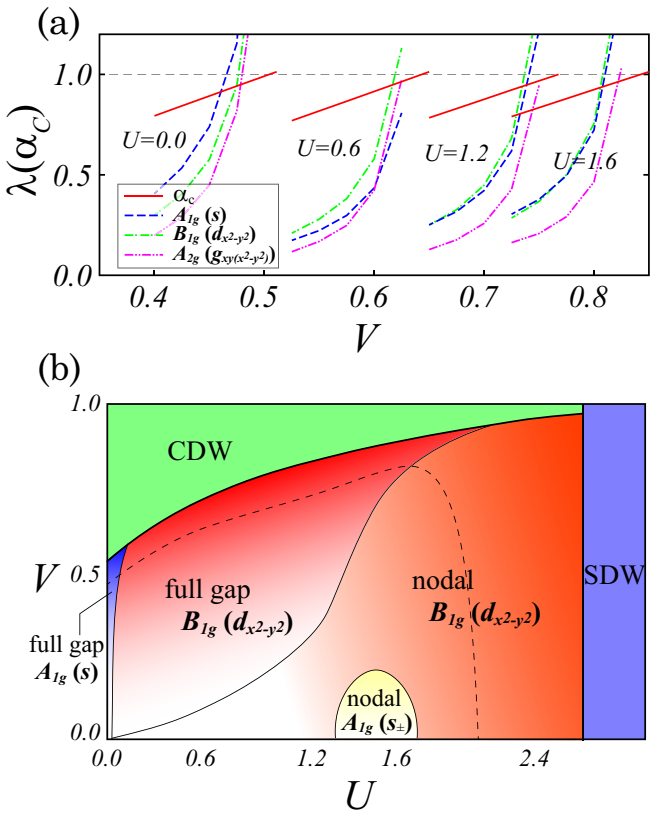

FIG. 3. (a) Stoner factor α_C and eigenvalue λ of each pairing symmetry as a function of V for several U. (b) $U-V$ phase diagram. The broken line corresponds to a phase transition line of $\lambda = 1$.

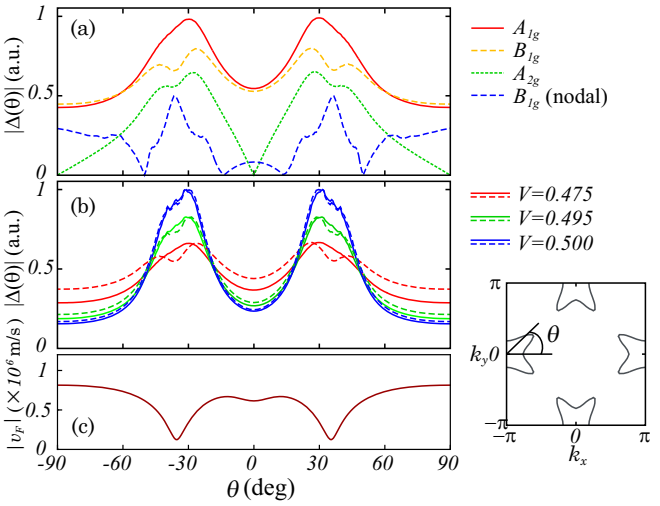

FIG. 4. (a) Superconducting gap $|\Delta(\theta)|$ on the Fermi surface. The angle θ is indicated in the right bottom inset. (b) Development of gap anisotropy in the fully gapped A_{1g} and B_{1g} states at $U = 0$. (c) Anisotropy of the Fermi velocity $|v_F(\theta)|$.

partly lifted, and then we obtain simple gap structures, i.e., the fully gapped s-wave A_{1g} state in Fig. 2(f), the $d_{x^2-y^2}$-wave B_{1g} state in Fig. 2(g), and the $g_{xy(x^2-y^2)}$-wave A_{2g} state in Fig. 2(h). Interestingly, due to the smallness of the Fermi pocket, the $d_{x^2-y^2}$-wave B_{1g} state is fully gapped, and the $g_{xy(x^2-y^2)}$-wave A_{2g} state has d_{xy}-type line nodes on the Fermi surface. The leading pairing state is an s-wave A_{1g} state with $\lambda = 1.15$. However, with a small but finite U, the leading pairing state becomes the fully gapped $d_{x^2-y^2}$-wave B_{1g} state. The eigenvalue $\lambda = 0.94$ for the B_{1g} state is slightly larger than $\lambda = 0.82$ for the A_{2g} state due to the presence of small repulsive interactions developing around $Q = (\pi/2, 0)$ and the equivalent Q vectors (not shown).

B. Phase diagram

In Fig. 3(a), we show eigenvalues as a function of V for several U along with α_c, which is a measure of the Stoner factor for the charge susceptibility χ_c. We can see that when α_c is enhanced as increasing V, eigenvalues λ are also enhanced and greater than 1 in a close proximity to the phase boundary of the charge density wave (CDW) at $\alpha_c = 1$. The leading pairing state is an s-wave A_{1g} state at $U = 0.0$, but a $d_{x^2-y^2}$-wave B_{1g} state for finite U. As U increases, the difference between A_{1g} and B_{1g} shrinks, and then these are nearly degenerate at $U = 1.6$. Since these fully gapped states have almost the same gap structure on the Fermi surface except for the sign, it is reasonable that these are nearly degenerate. For $U > 1.6$, the dominant fluctuation changes from the ferroic charge fluctuation into the incommensurate spin fluctuation. The leading pairing state is a nodal $d_{x^2-y^2}$ wave state in Fig. 2(c). These are summarized in the phase diagram of Fig. 3(b). We conclude that the fully gapped superconductivity driven by the ferroic charge fluctuation appears near the CDW phase boundary, while the magnetically driven nodal $d_{x^2-y^2}$-wave state appears near the spin density wave (SDW) phase boundary.

C. Gap anisotropy

Recent experimental observations have implied the strong gap anisotropy in this material [27]. Here, let us dissect the gap anisotropy on the Fermi surface for the obtained gap structures. Figure 4(a) depicts the angle dependence of gap amplitude $|\Delta(\theta)|$ on the Fermi surface for possible gap structures. Roughly speaking, the gap amplitude is enhanced at around $\theta \sim 30^\circ$, independent of the gap symmetry. This also corresponds to bright spots at the corner of the Fermi pocket in the gap structure of Fig. 2. Such features are related to strong suppression of the Fermi velocity. Now, let us move to the details of each gap structure.

The A_{2g} state in Fig. 2(h), which does not appear in the phase diagram of Fig. 3(b), has d_{xy}-like symmetry-protected nodes. The fully gapped A_{1g}/B_{1g} state in Fig. 2(f)/2(g) also has d_{xy}-like anisotropy, although the gap at $\theta = 0^\circ$ and $\pm 90^\circ$ is a finite gap minima, not a gap zero. As indicated in Fig. 4(b), such anisotropy develops in the close proximity to a CDW phase boundary. The nodal B_{1g} in Fig. 2(c) has fine structure, where the nodal positions are located at $\theta \sim \pm 15^\circ$ and $\pm 50^\circ$. Experimentally, the recent ARPES data shows a gap node/minimum at $\theta = 0$, but its data is scattered at around $\theta = 90$. Then, at least, the behavior at around $\theta = 0$ is consistent with the d_{xy}-like gap anisotropy. However, the symmetry-protected nodes in the A_{2g} state, which cannot be easily lifted, are incompatible with the fully gapped nature

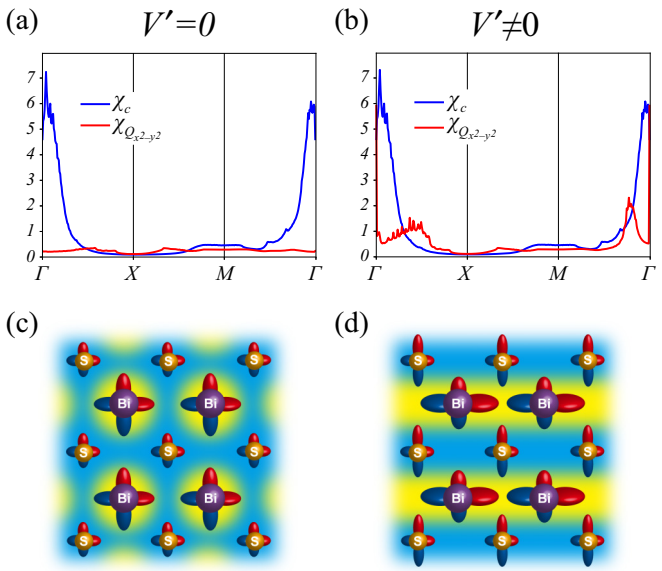

FIG. 5. Charge and quadrupole susceptibilities (χ_C/χ_Q) at (a) $(U,V,V') = (0.0,0.475,0.0)$ eV and (b) $(U,V,V') = (0.0,0.475,1.22)$ eV. Schematic charge distribution of the (c) ferroic charge ordering and (d) quadrupole ordering.

reported by some experiments [23,24]. Thus, the fully gapped A_{1g} or B_{1g} state is a possible gap structure in this system. In particular, the latter fully gapped $d_{x^2-y^2}$-wave B_{1g} state is stable in the wide range of the phase diagram. Also, the anisotropy on the Fermi surface is partially consistent with the recent ARPES data. This state is mediated by the ferroic charge fluctuation, which is driven by the intersite interactions between the Bi and S atom.

D. Charge and quadrupole ordering

Finally, let us discuss possible charge and quadrupole ordering. As mentioned above, the intersite interaction V between Bi and S atoms leads to the ferroic charge fluctuation. As indicated in Fig. 5(a), its net component is the charge (electric monopole) fluctuation, defined by $\chi_c = \sum_l \chi_{llll} + \sum_{l\neq m} \chi_{llmm}$. In general, the intersite interactions are orbital dependent, that is to say, $V' \neq 0$. As indicated in Fig. 5(b), with increasing the difference V', the Q_{22}-type quadrupole fluctuation, $\chi_Q = \sum_l \chi_{llll} - \sum_{l\neq m} \chi_{llmm}$, is enhanced, and then the fully gapped B_{1g} state is more stable (not shown). The corresponding order is a stripe-type orbital ordering, as illustrated in Fig. 5(d). This orbital ordering may correspond to checkerboard-stripe charge order, observed by STM/STS [28]. Note that $V - V' < 0$ in this region. It implies that the intersite attractive force may be important in the emergence of checkerboard-stripe charge order. Therefore, it may be difficult to understand it in terms of purely electronic interactions.

IV. CONCLUSION

In the present study, we studied the superconducting gap anisotropy in the BiS_2-based superconductors. We constructed the first-principles downfolded band structure on the basis of Bi $6p_x/p_y$ and S $3p_x/p_y$ orbitals on a BiS_2 single layer. In the extended Hubbard model with the intersite interactions between the Bi and S atoms, we found that the ferroic charge and quadrupole fluctuations can be enhanced. This may be related to the observation of checkerboard-stripe charge order. Such charge and quadrupole fluctuations lead to the fully gapped $d_{x^2-y^2}$-wave pairing state. The obtained gap amplitude has d_{xy}-like anisotropy on a Fermi surface, although the gap at $\theta = 0^\circ$ and $\pm 90^\circ$ is a finite gap minima, not a gap zero. Such anisotropy is partially consistent with the recent experimental observations. These results indicate that the intersite interactions are the key ingredients to understand the superconductivity in this system.

ACKNOWLEDGMENTS

We acknowledge Y. Ota, K. Okazaki, and S. Shin for the recent ARPES data, and thank T. Nomoto and K. Hattori for valuable comments. This work was partly supported by JSPS KAKENHI Grants No. 16H04021, No. 16H01081, No. 15H05745, No. 15H02014, and No. 25009605.

[1] Y. Mizuguchi, H. Fujihisa, Y. Gotoh, K. Suzuki, H. Usui, K. Kuroki, S. Demura, Y. Takano, H. Izawa, and O. Miura, Phys. Rev. B **86**, 220510(R) (2012).
[2] Y. Mizuguchi, S. Demura, K. Deguchi, Y. Takano, H. Fujihisa, Y. Gotoh, H. Izawa, and O. Miura, J. Phys. Soc. Jpn. **81**, 114725 (2012).
[3] R. Jha, A. Kumar, S. K. Singh, and V. P. S. Awana, J. Appl. Phys. **113**, 056102 (2013).
[4] R. Céolin and N. Rodier, Acta Crystallogr. Sect. B **32**, 1476 (1976).
[5] H.-F. Zhai, P. Zhang, S.-Q. Wu, C.-Y. He, Z.-T. Tang, H. Jiang, Y.-L. Sun, J.-K. Bao, I. Nowik, I. Felner, Y.-W. Zeng, Y.-K. Li, X.-F. Xu, Q. Tao, Z.-A. Xu, and G.-H. Cao, J. Am. Chem. Soc. **136**, 15386 (2014).
[6] R. Jha, A. Kumar, S. K. Singh, and V. Awana, J. Supercond. Novel Magn. **26**, 499 (2013).
[7] Y. Kamihara, T. Watanabe, M. Hirano, and H. Hosono, J. Am. Chem. Soc. **130**, 3296 (2008).
[8] Y. Fuseya, M. Ogata, and H. Fukuyama, J. Phys. Soc. Jpn. **84**, 012001 (2015).
[9] H. Kotegawa, S. Nakahara, H. Tou, and H. Sugawara, J. Phys. Soc. Jpn. **83**, 093702 (2014).
[10] R. Troć and V. Tran, J. Magn. Magn. Mater. **73**, 389 (1988).
[11] *Non-Centrosymmetric Superconductors Introduction and Overview*, Lecture Notes in Physics, edited by E. Bauer and M. Sigrist (Springer, New York, 2012).
[12] B. Li, Z. W. Xing, and G. Q. Huang, Europhys. Lett. **101**, 47002 (2013).

[13] X. Wan, H.-C. Ding, S. Y. Savrasov, and C.-G. Duan, Phys. Rev. B **87**, 115124 (2013).
[14] T. Yildirim, Phys. Rev. B **87**, 020506 (2013).
[15] X. Wu, J. Yuan, Y. Liang, H. Fan, and J. Hu, Europhys. Lett. **108**, 27006 (2014).
[16] H. Usui, K. Suzuki, and K. Kuroki, Phys. Rev. B **86**, 220501(R) (2012).
[17] G. B. Martins, A. Moreo, and E. Dagotto, Phys. Rev. B **87**, 081102 (2013).
[18] T. Agatsuma and T. Hotta, J. Magn. Magn. Mater. **400**, 73 (2016).
[19] C.-L. Dai, Y. Yang, W.-S. Wang, and Q.-H. Wang, Phys. Rev. B **91**, 024512 (2015).
[20] C. Morice, R. Akashi, T. Koretsune, S. S. Saxena, and R. Arita, Phys. Rev. B **95**, 180505 (2017).
[21] Y. Liang, X. Wu, W.-F. Tsai, and J. Hu, Front. Phys. **9**, 194 (2014).
[22] H. Usui and K. Kuroki, Nov. Supercond. Mater. **1**, 50 (2015).
[23] L. Jiao, Z. Weng, J. Liu, J. Zhang, G. Pang, C. Guo, F. Gao, X. Zhu, H.-H. Wen, and H. Q. Yuan, J. Phys.: Condens. Matter **27**, 225701 (2015).
[24] T. Yamashita, Y. Tokiwa, D. Terazawa, M. Nagao, S. Watauchi, I. Tanaka, T. Terashima, and Y. Matsuda, J. Phys. Soc. Jpn. **85**, 073707 (2016).
[25] M. Aslam, S. Gayen, A. Singh, M. Tanaka, T. Yamaki, Y. Takano, and G. Sheet, arXiv:1604.06325.
[26] J. Zhang, K. Huang, Z. F. Ding, D. E. MacLaughlin, O. O. Bernal, P.-C. Ho, C. Tan, X. Liu, D. Yazici, M. B. Maple, and L. Shu, Phys. Rev. B **94**, 224502 (2016).
[27] Y. Ota, K. Okazaki, H. Q. Yamamoto, T. Yamamoto, S. Watanabe, C. Chen, M. Nagao, S. Watauchi, I. Tanaka, Y. Takano, and S. Shin, Phys. Rev. Lett. **118**, 167002 (2017).
[28] T. Machida, Y. Fujisawa, M. Nagao, S. Demura, K. Deguchi, Y. Mizuguchi, Y. Takano, and H. Sakata, J. Phys. Soc. Jpn. **83**, 113701 (2014).
[29] P. Blaha, K. Schwarz, P. Sorantin, and S. Trickey, Comput. Phys. Commun. **59**, 399 (1990).
[30] N. Marzari and D. Vanderbilt, Phys. Rev. B **56**, 12847 (1997); I. Souza, N. Marzari, and D. Vanderbilt, *ibid.* **65**, 035109 (2001). The Wannier functions are generated by the code developed by A. A. Mostofi, J. R. Yates, N. Marzari, I. Souza, and D. Vanderbilt, Comput. Phys. Commun. **185**, 2309 (2014), http://www.wannier.org/.
[31] J. Kunes, R. Arita, P. Wissgott, A. Toschi, H. Ikeda, and K. Held, Comput. Phys. Commun. **181**, 1888 (2010).
[32] J. P. Perdew, A. Ruzsinszky, G. I. Csonka, O. A. Vydrov, G. E. Scuseria, L. A. Constantin, X. Zhou, and K. Burke, Phys. Rev. Lett. **100**, 136406 (2008).
[33] This four-orbital model Hamiltonian is licensed under CC BY 4.0 on GitHub; https://github.com/ktszk/ham_data.
[34] T. Takimoto, T. Hotta, and K. Ueda, Phys. Rev. B **69**, 104504 (2004).